19th Brazilian Congress of Thermal Sciences and Engineering
November 6th–10th, 2022, Bento Gonçalves - RS - Brazil

# ENCIT2022-0063
# VALIDATION OF A LOW-COST IMU FOR VIBRATION TRACKING ALONG OFFSHORE LINE MODELS

**Aline Peres Leal**
Polytechnic School of University of São Paulo, São Paulo - Brazil
aline.peresleal@usp.br

**Rafael D Amaro Chiara**
**Monique Ellen Bruner**
**André Luís Condino Fujarra**
University of Santa Catarina, Jonville Technological Center, Joinville - Brazil
rafael.chiara@grad.ufsc.br
monique.bruner@posgrad.ufsc.br
andre.fujarra@ufsc.br

***Abstract.*** *It is known that field measurement of offshore structures is highly dependent on environmental conditions, availability and accuracy of applied equipment, and external interference, among other aspects. Currently, the cost to reliably predict displacements and frequencies of risers, umbilicals, or mooring lines is very high. Alternatively, careful signal treatments and validation studies are required to obtain good results through low-cost solutions. In order to seek a solution of the latter nature, this work aims to carry out experimental studies related to an embedded vertical tube using an inertial measurement unit (IMU) to track the movement of some discrete points along the length. Different positions and initial excitation are tested to validate the IMU readings against those obtained by an optical tracking system used as a reference. The aluminum tube is filled with sand to lower the natural frequency values. The IMU comprises three-axis accelerometers, rate gyroscopes, and magnetometers, from which the angles are obtained indirectly through the Kalman filter to build the rotation quaternion at each time step. Thus, the acceleration vector can be rotated to a fixed coordinate system, north-east-down (NED) frame, to be represented locally. The double integration of the acceleration vector is studied, filtering out noise and drift problems to calculate the tube displacements. The amplitudes and frequencies obtained by the IMU are compared to those from the optical tracking system, composed of five cameras tracking reflective targets.*
***Keywords:*** *Inertial Measurement Unit (IMU), tracking vibration, experimental validation, digital filtering, signal processing.*

## 1. INTRODUCTION

Risers, umbilicals, mooring lines, and other submerged cables undergo the flow-induced vibration (FIV) phenomenon. Monitoring these systems can be complicated and currently involves expensive instruments and the usage of robots. Vibration investigations comprise analysis of natural frequencies, damping factors, and damped natural frequencies, being free vibration studies essential to determine these parameters. Then, forces involved in the vibration induced by the flow are related to the structure's natural parameters to investigate the response regime.

An approach to estimate the modal shape and frequencies excited on flexible cables is the modal reconstruction. Researches have been applying multiple sensors along the cable to monitor the displacement over time. Usually, the sensors used are strain gauges, optical fiber, accelerometers, and/or rate gyros (Mukundan *et al.*, 2010; McNeill, 2012; Li *et al.*, 2019). These works analyzed the results for well-known sensors positions aligned to cross and in-line flow.

Using only empirical methods, Shi *et al.* (2010) estimate the response in VIV using only the riser response data, usually obtained by strain gauges and accelerometers. The methods weighted waveform analysis (WWA), proper orthogonal decomposition (POD), modal phase reconstruction (MPR), modified WWA procedure, hybrid method (combination of MPR and the modified WWA) are convenient to estimate fatigue damage rates reliably.

Mukundan *et al.* (2010) studied the reconstruction of the riser motion from a minimal number of strain gauges placed along the tube. The reconstruction accuracy using few sensors depends on the peak response modes and frequencies

estimation, which means knowing the flow profile.

In the studies of McNeill (2012), to estimate the stress spectral automoments along the riser using accelerometers and rate gyros data, spectral methods were used. These methods were applied to simulated VIV data (from a deep-water riser) and measured VIV data (from a model test of a slender and uniform riser). ROV was used for installing data loggers. The method could determine VIV fatigue damage and, a relevant error value was observed in the asynchronous data, however.

Changing the type of sensor, Li *et al.* (2019) investigated deep-sea riser vibration by using Bare Fiber Bragg Grating (BFBG) sensor technology. This technology enables the calculation of riser's displacement over time, vibration amplitude and frequency in a accurate manner, although it requires careful installation.

In this context, there is a study gap of sensors installed in positions not well known, which is the case of sensors placed, for example, without the precise control of a robot or before risers installation.

Low-cost sensors present readings carrying considerable bias and noise values. To make possible the application of these measurement units, errors must be filtered and treated. Bias, scale factor, and non-orthogonality are the main errors that can be investigated in a calibration process for accelerometers, rate gyros, and magnetometers. Signal analysis is essential for reliable results, making validation process possible.

Vissière *et al.* (2007) analyzed magnetometers to determine position estimation for a rigid body using an inertial measurement unit (IMU) and a set of magnetometers. The authors related the importance of magnetic field when the Global Positioning System (GPS) is unavailable. The displacement results in the tri-dimensional space were identified, but the accuracy needed to be improved.

Driessen *et al.* (2018) studied sensor-fusion to determine velocity, position, and attitude for an unmanned aerial vehicle (UAV). They used an ensemble composed by an IMU and an optical-flow sensor, including a sonar and an extra gyroscope. The UAV's parameters could be estimated without drift, with slight magnitude difference.

Within this frame of reference, the present work aims to validate, for an embedded vertical tube, displacement, orientation, frequencies, and damping factor computed through IMU readings, contrasting the results with an optical system. The experimental studies were carried out including signal treatment with sensor-fusion and band-pass filter.

## 2. INERTIAL MEASUREMENT UNIT

Inertial sensors have this denomination because they are based on inertia measuring principles. Accelerometers use gravitational acceleration vector to compute the gravitational force acting on the body. Rate gyros, usually called gyroscopes, act according to angular momentum conservation.

The inertial sensor market is broad, and the performance characteristics vary according to the sensor's grade and cost. Micro Electro-Mechanical System (MEMS) inertial sensors are composed of a suspended mass between a pair of capacitive plates; they are less expensive, although present considerable bias stability.

The nomenclature Inertial Measurement Unit (IMU) describes a set of gyroscopes, accelerometers, and magnetometers with no navigation outputs, being the magnetometers optional. The user must treat the raw data from these sensors.

## 3. CALIBRATION

### 3.1 Accelerometers and Rate gyros

The accelerometer calibration was conducted according to the process proposed by Zhang *et al.* (2008), a multi-position calibration. The multi-position method uses the norm of the static reading, so the gravity acceleration is the reference.

The calibration can be conducted in the field without any high-precise instruments. The three-axis accelerometer is left in different static positions. According to the relations with gravitational acceleration value, Eq. 1, the bias, scale factor, and misalignment errors can be estimated.

$$\begin{aligned} |g^n|^2 &= \left[N_x^2 \;\; N_y^2 \;\; N_z^2 \;\; 2N_xN_y \;\; 2N_xN_z \;\; 2N_yN_z \;\; -2N_x \;\; -2N_y \;\; -2N_z \;\; 1\right] \\ &\quad . \left[k_{11}^A \;\; k_{22}^A \;\; k_{33}^A \;\; k_{12}^A \;\; k_{13}^A \;\; k_{23}^A \;\; k_{14}^A \;\; k_{24}^A \;\; k_{34}^A \;\; k_{44}^A\right]^T + \Delta \\ &= N_v.K_v + \Delta \end{aligned} \tag{1}$$

where $N_v$ is defined as a vector constructed by elements of $N$ (accelerometer readings) and $K_v$ is a vector constructed by 10 different elements of $K^A$.

For that, the IMU was left 1 minute in each of the 18 static positions, using an acrylic box, as shown in Fig. 1. The IMU was fixed in the box bottom; then, the box was rotated and placed in different positions. According to Zhang *et al.* (2008), the angles do not need to be precise; only present variation among them once the norm of the accelerometer outputs is used, which is equal to the magnitude of referenced gravity. The mean values of each reading position are used to compose the $N$ matrix.

Estimating $K_v$ by the least square algorithm on Octave software, it was possible to calculate the matrix $K^a$ and the

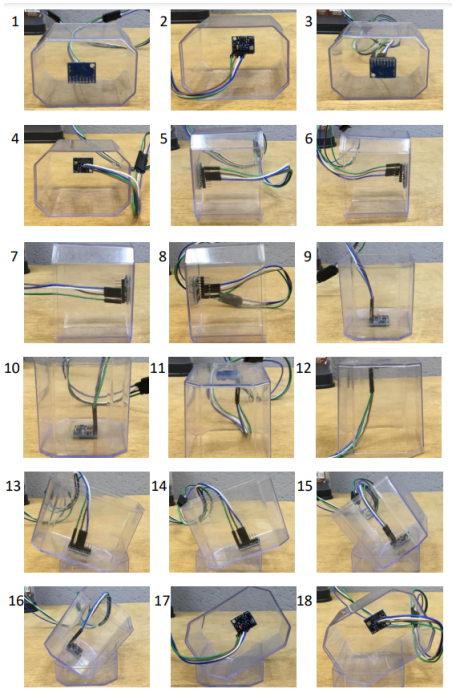

Figure 1: IMU static positions for calibration.

vector $f_0$, being $f_0$ the accelerometer's bias and $K^a$ a matrix encoding scale factors and nonorthogonalities. Then, the outputs of the accelerometers can be transformed into specific force in the body frame by:

$$f^b = K^a N - f_0 - \delta_f \tag{2}$$

where $\delta_f$ is the signal noise.

As the readings are for static IMU, 3-axis rate gyros bias can also be calculated, once these values need to be zero.

### 3.2 Magnetometers

For the magnetometer calibration, the ellipsoid fit was applied. It is known that the Earth's magnetic field has a spherical shape, without hard and soft iron errors. Using the least square algorithm in the data points captured by rotating the IMU, the center (offsets) and rotation matrix can be found to transform the magnetic reading to a zero-centered sphere.

The algorithm fits an ellispoid in the form $Ax^2 + By^2 + Cz^2 + 2Dxy + 2Exz + 2Fyz + 2Gx + 2Hy + 2Iz + J = 0$ to the set of xyz data points.

Having the vector of center values/offsets ($o_m$) and the rotation matrix ($R_m$) estimated, the correction in the magnetometers readings is calculated by:

$$m_c = R_m.(m_a - o_m) \tag{3}$$

where $m_c$ is the vector representing the corrected values of the magnetometers axes and $m_a$ the vector containing the magnetometers readings.

Both calibration processes were conducted in two different test days to confirm the parameters.

## 4. EXPERIMENTAL SETUP

The experiments were conducted in the Modeling and Data Analysis Laboratory (LabMAD) at the Federal University of Santa Catarina (UFSC). The aluminum cylinder, with 1.22 mm thickness, an external diameter of 25.73 mm, and 2580 mm length, was embedded and filled with sand to lower its natural frequency. A support for vertical fixation of the tube was then used to have the embedded condition fixed with parabolts to the floor. In the fixed base, a piece of wood was used to prevent the tube from deforming when fixing the support, see Figure 2. The final setup, painted in black to avoid refection to the tracking system, is shown in Figure 3.

The Optitrack, an optical tracking system, was used to validate the IMU readings. A five-camera set was mounted on a metallic structure on the walls, see Fig. 4. The camera calibration is necessary, where the wanding process was started without any reflective objects, capturing points of the test area. With that, the uncertainty of the reading was calculated, and the origin of the coordinates was set. Then, reflective targets were placed in the tube, fixing support, floor,

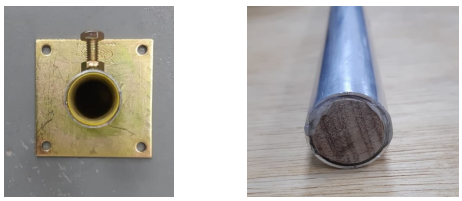

(a) Base for fixing. (b) Wood piece.

Figure 2: Fixation used.

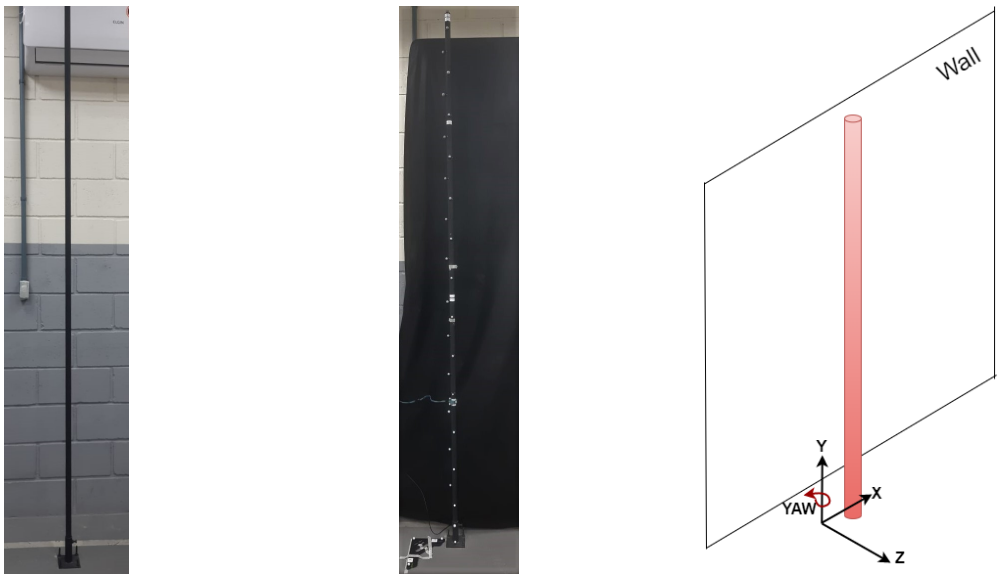


(a) Final embedded cylinder setup. (b) Markers located. (c) Optitrack's coordinate system.

Figure 3: Final setup configuration

and IMU. The Optitrack's coordinated system is illustrated in Fig. 3c, with the x-axis pointing to the left side, the y-axis pointing to the cylinder length, and the z-axis to the front of the image. The angular rotation on the horizontal plane is indicated by the yaw angle, also known as azimuth or heading. The cameras captured the displacement of the targets at an acquisition frequency of 100Hz, using Motive software to display and record the results. For the IMU position, the rigid body property in Motive was used, having results of translation and rotation.

Regarding the IMU, the program to read the sensor's raw values was programmed on the Arduino Uno R3 board, powered via a USB cable connected to the GY-87 module through jumpers. The data was saved on an SD card with a frequency of approximately 100Hz. The IMU was situated in a plastic clamp to maintain a known position during each test, see Fig. 5.

This setup used different factors and levels to conduct the tests, as presented in Tab. 1. The variations have the function of showing how results can be reliable, regardless of position. With the repetitions, uncertainty and standard deviation could be computed. Also, a zero test was conducted each day, having the IMU in the same position to ensure the systems were stable on time.

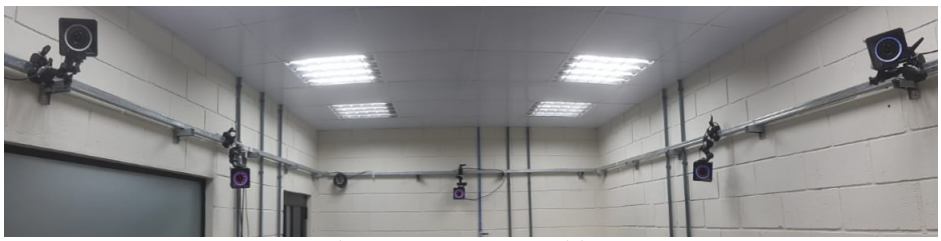

Figure 4: Cameras position.

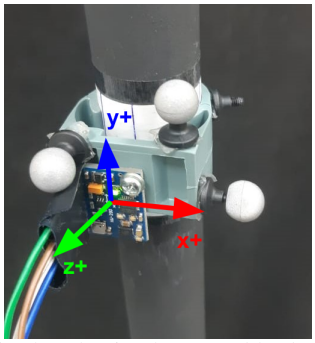

Figure 5: IMU fixed in the plastic clamp and body frame representation.

## 5. SIGNAL ANALYSIS

Optitrack system results for each marker were separeted by columns. Possible spikes were removed using median filter of three elements and, a find nonzero function used to clear away instants of time when targets vanish.

Raw values from the IMU sensors were recorded, then signal treatment was conducted in Octave numerical computation software. Calibration factors and sensitivity factors were applied.

To modify the results in IMU/body frame ($^b$) to the Optitrack frame ($^{op}$), making possible the comparison, it is necessary to apply the rotation. Roll ($\phi$) and pitch ($\theta$) angles are calculated through accelerations as demonstrated in Groves (2013),

$$\phi = atan2\left(a_y, a_z\right); \tag{4}$$

$$\theta = atan2\left(a_x, \sqrt{a_y^2 + a_z^2}\right); \tag{5}$$

in radians. The heading (or yaw) angle is calculated by the 3-axis magnetometer using the following relation:

$$\psi_m = atan2\left\{-M_y cos\phi + M_z sin\phi, M_x cos\theta + M_y sin\phi sin\theta + M_z cos\phi)sin\theta\right\}; \tag{6}$$

in radians.

Also, integration from the rate gyros gives the instantaneous angles. Sensor fusion was used to reduce drift problems from time integration and high-frequency noise from the accelerometer and magnetometer. This fusion was conducted using the Kalman filter.

Kalman filter estimates quantities using all readings of the sensor axis contributions in the IMU. The first estimation is given by the rate gyros, while the second estimation generated by the navigation aid sensors, accelerometers for roll and pitch, and magnetometers for yaw angles.

| **Factors** | **Levels** | **Tests nomeclature** |
|---|---|---|
| Position along the cylinder | 2.560 m | L01 |
| | 1.20 m | L12 |
| | 0.645 m | L14 |
| Heading | 0 ° | yaw000 |
| | 45 ° | yaw045 |
| | 90 ° | yaw090 |
| | 135 ° | yaw135 |
| Initial excitation | static | m0 |
| | deflection on the top | m1 |
| | deflection in the middle | m2 |
| IMU axes | y-axis up | yc |
| | y-axis down | yb |
| Repetitions | 5 | r_001,2,3,4,5 |
| Total of tests | 360 | |

Table 1: Test matrix.

The system state matrix at time $k$ is given by:

$$x_k = \begin{bmatrix} \Theta \\ \mathrm{b} \end{bmatrix} = Fx_{k-1} + Bu_k + w_k \tag{7}$$

$$z_k = Hx_k + v_k \tag{8}$$

where $\Theta$ is the angle considered (roll, pitch or yaw) and $b$ the rate gyro drift bias, $w_k$ is a process noise and $v_k$ is a measurement noise, $u_k$ is the control input, given by the rate gyro signal. The matrix $F$ is called state transition matrix.

Also, $z_k$ is the measurement output and $H$ is the measurement matrix. As the measurement is from the accelerometers/magnetometers, $H$ is defined as:

$$H = [1 \;\; 0] \tag{9}$$

The prediction step of the state at time $t_{k+1}$is given by:

$$x_{k+1/k} = F_k x_{k/k} + b\omega_{k+1} \tag{10}$$

The covariance matrix is predicted forward in time using the following equation:

$$P_{k+1/k} = F_k P_{k/k} F_k^T + Q \tag{11}$$

$P_{k+1/k}$ is the expected value of the covariance matrix at time $t_{k+1}$ predicted at time $t_k$. $Q$, the system noise matrix, is set up according to the expected level of noise on the sensors.

In the measurement update step, the estimates of the errors in the system states are computed using:

$$x_{k+1/k+1} = K_{k+1} y_{k+1} \tag{12}$$

being $y_{k+1}$ given by:

$$y_{k+1} = z_{k+1} - Hx_{k+1/k} \tag{13}$$

and the covariance matrix is updated as:

$$P_{k+1/k+1} = [I - K_{k+1} H_{k+1}] P_{k+1/k} \tag{14}$$

The Kalman gain $K$ is calculated as:

$$K_{k+1} = P_{k+1/k+1} H_{k+1}^T [H_{k+1} P_{k+1/k} H_{k+1}^T + R]^{-1} \tag{15}$$

where $R$ is the measurement noise matrix.

Then, at each time step, the rotation is computed using quaternions, Eq. 16, written according to the Euler angles $\phi$, $\theta$ and $\psi$:

$$q = [q_w \;\; q_x \;\; q_y \;\; q_z]^T \tag{16}$$

where,

$$\begin{aligned} q_w &= c\frac{\phi}{2}c\frac{\theta}{2}c\frac{\psi}{2} + s\frac{\phi}{2}s\frac{\theta}{2}s\frac{\psi}{2} \\ q_x &= s\frac{\phi}{2}c\frac{\theta}{2}c\frac{\psi}{2} - c\frac{\phi}{2}s\frac{\theta}{2}s\psi/2 \\ q_y &= c\frac{\phi}{2}s\frac{\theta}{2}c\frac{\psi}{2} + s\frac{\phi}{2}c\frac{\theta}{2}s\frac{\psi}{2} \\ q_z &= c\frac{\phi}{2}c\frac{\theta}{2}s\frac{\psi}{2} - s\frac{\phi}{2}s\frac{\theta}{2}c\psi/2 \end{aligned} \tag{17}$$

being $c$ and $s$ cos and sin, respectively.

Titterton *et al.* (2004) indicated that quaternion attitude representation allows a transformation from one coordinate frame to another, using a single rotation about a vector. The rotation quaternion is represented by Eq. 18:

$$q = [cos(\mu/2), (\mu_x \vec{i}, \mu_y \vec{j}, \mu_z \vec{k}) sin(\mu/2)] \tag{18}$$

where $\mu_x$, $\mu_y$, $\mu_z$ are the components of the angle vector and $\mu$ the magnitude.

The vector rotation using quaternion is calculated by:

$$p' = qpq^* \tag{19}$$

where $q^*$ is the complex conjugate. The rotated coordinates from $p'$ are extracted from the imaginary part once the real element is always equal to zero. This transformation results in north, east, and down (NED) coordinates. To rotate to the Optitrack frame, a new rotation is made only around the down axis, according to the angle related to the $x_{op}$ axis.

Next, a sixth-order high pass Butterworth filter was applied to the acceleration vector to reduce drift related to the integration process. The integration using the trapezoid method integral is conducted and the Butterworth filter, using cut frequencies of 0.95 and 15 Hz applied to the velocities vectors. The same is done to obtain the displacement results. Then, the displacements in the xyz system of Optitrack were compared.

Fast Fourier Transform (FFT) was used to analyze the frequencies, considering more than 30 vibration cycles. Peak frequencies were collected to recognize the occurrence of each mode. To avoid the aliasing problem, Nyquist frequency was observed.

The damping factor was calculated using the logarithmic decrement, which represents how the amplitude of a free damped vibration decreases.

$$\delta = log\left(\frac{x_n}{x_{n+1}}\right) \tag{20}$$

Logarithmic decrement was computed as the mean value for at least 10 cycles, than, the damping factor estimated as:

$$\zeta = \frac{\delta}{\sqrt{4\pi^2 + \delta^2}} \tag{21}$$

In summary, the process of the present data analysis is shown in Fig.6.

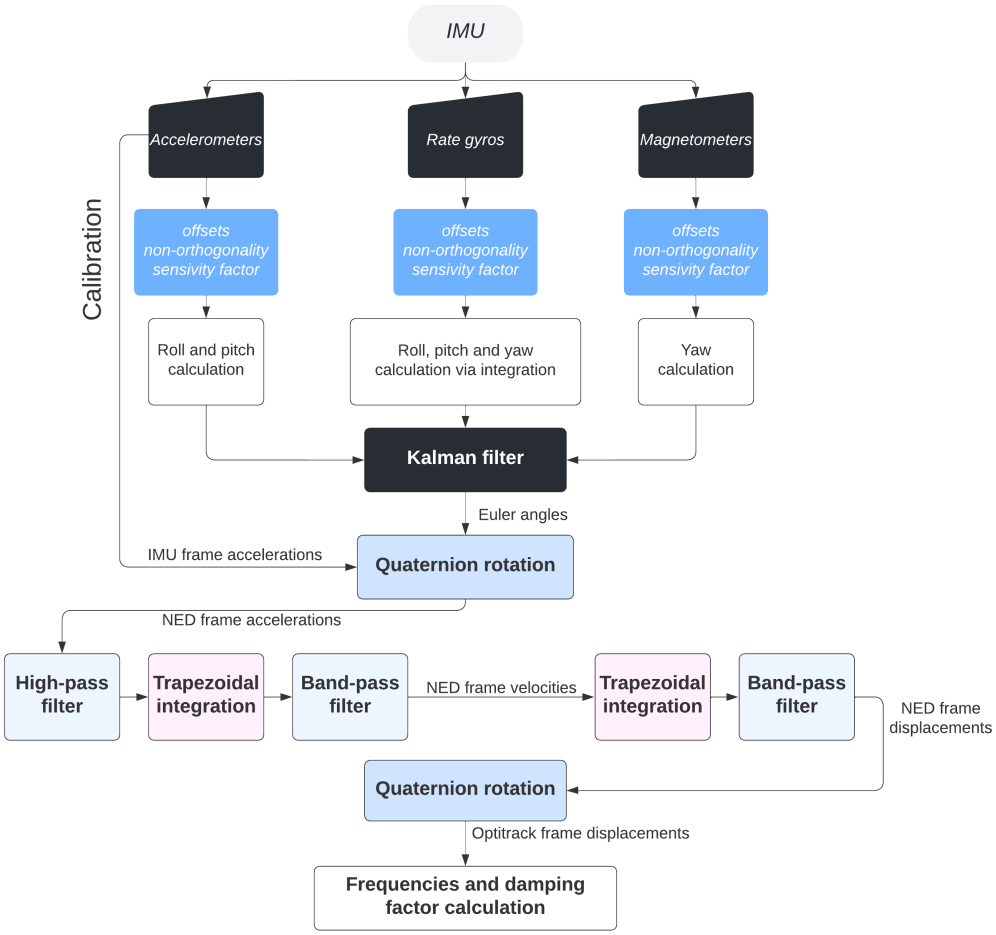


Figure 6: Signal analysis flowchart.

## 6. RESULTS AND DISCUSSIONS

The key results of this experimental study are frequency and damping factor obtained by two systems, which are compared and summarized in graphics. Time history for amplitude displacement is shown for some tests to demonstrate the agreement between readings.

The temperature in the test room was controlled and read by the IMU. Values between 21 and 24°C were found for all tests. Magnetometer calibration results show a zero centered sphere, Fig. 7. Accelerometer calibration results gave offsets and rotation matrix values to compensate axis misalignment.

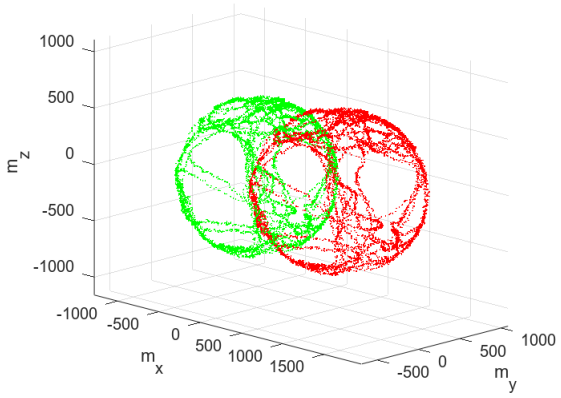


Figure 7: Magnetometers readings before (red) and after(green) calibration.

For the zero tests, the marker positions obtained by the optical system were the same, as can be seen in Fig. 8a, being the three first markers belonging to the rigid body and the other ones to the cylinder. Concerning the IMU, the orientation was considered and the readings are presented in Fig. 8b. Hereupon, the system stability over time is noted.

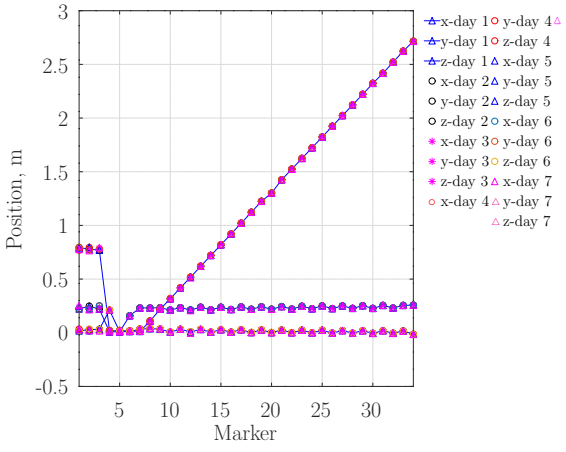


(a) Marker positions.

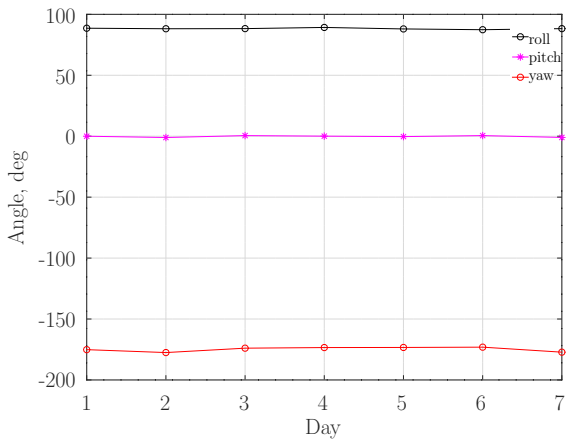


(b) IMU angles.

Figure 8: Sensors situation on the test days.

Since each test condition was repeated five times, the mean and time standard deviation for each static test (m0) were computed, Fig. 9. Red and blue bars represent IMU and Optitrack results, respectively. The average over time with the Optitrack system were computed removing the initial static position, related to the origin of coordinate system. The averages using IMU are very close to zero once pass band filter attenuates values with very low frequency, which is related to the signal average. IMU standard deviations are larger, however, generally do not exceed values of 0.0001m, or 0.1mm. For Fig. 9b, one test in 90° presented a standard deviation a barely greater than 0.0001m in the x-direction and Optitrack with more significant values in three situations. For Fig.9c the case in 90° also presented discrepancies. Variance observed in Optitrack data can occur due to the camera light overlay, causing slight jumps in position, moving the average to other values. This situation was observed and avoided whenever possible.

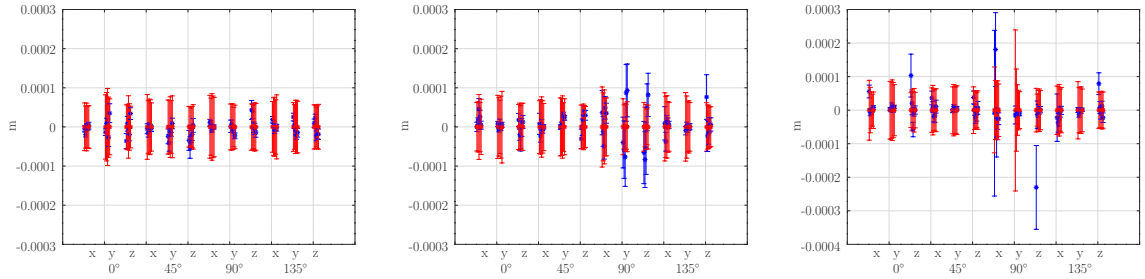


(a) $L14$ (b) $L12$ (c) $L01$

Figure 9: Time standard deviation for each static test replication, IMU results in red and Optitrack in blue.

Signals obtained from the IMU sensors are exemplified in Fig. 10. This case exhibit initial IMU angles equal to 87.28°, -0.12° and 176.99° for roll, pitch and yaw, respectively. At about 5 seconds, the initial excitation for the first mode (m1) was done. Gravity acceleration appears with a negative signal in the y-direction once y-axis points up. Due to small roll and pitch inclination, x and z accelerations are not around zero, which is corrected when the coordinates transformation is applied. Neither orientation nor acceleration present drift problems.

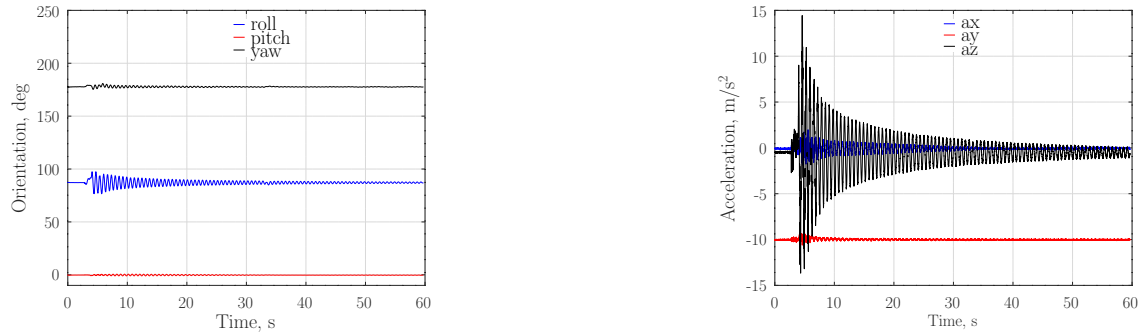


(a) Angles. (b) Accelerations

Figure 10: Readings in IMU frame, L01 and heading 0°.

According to the methodology, the IMU displacement was computed from the acceleration signals integrated twice in time. The main objective of this work is to see if this integration and coordinates transformation lead to reliable values when compared to the optical system. Figure 11a presents displacement values in the x-direction, same direction as the initial disturbance. Asterisks represent the points used to compute the damping factor. The agreement between the signals is noteworthy. Exponential decay and a well-defined frequency are seen.

Following, in Fig.11b, the relative angle between the IMU position and the Optitrack x-axis is 45°. After the signal treatment and frame rotation, clearly the displacements fit. In Fig. 11c the amplitudes are smaller than for L01 once this position is closer to the fixed side of the cylinder. With that, IMU results using the methodology applied in this work are independent of IMU orientation or position along the cylinder length.

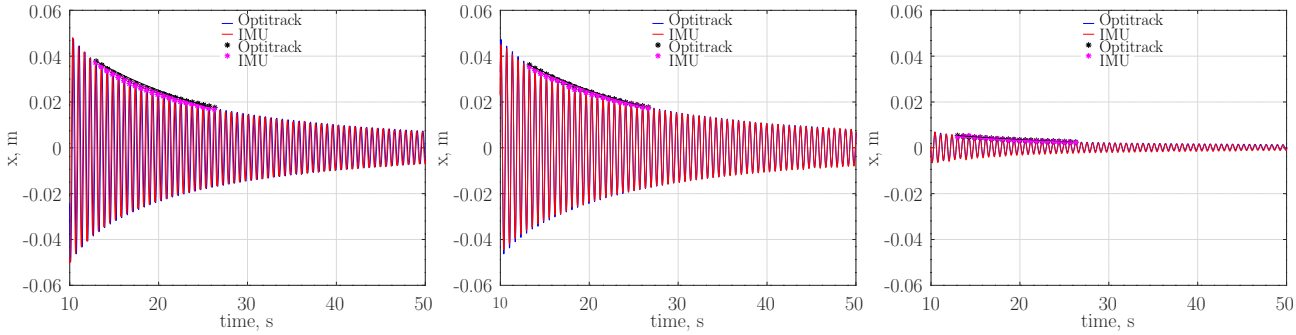


(a) L01, heading 0°. (b) L01, heading 45°. (c) L14, heading 45°.

Figure 11: IMU and rigid body displacement for excitation in $x$ direction.

Related to damped natural frequencies obtained for the first mode excitation (m1), the results are presented in terms

of repetition averages and standard deviation. For the L14 position, Fig. 12a, frequencies presented practically a constant difference of 0.022, equivalent to 1.37%; damping factor varies for both Optitrack and IMU, with values between 0.5% and 0.66%. For L12, Fig. 12b, the results present behavior similar to L14. Attention is given to results for L01, Fig. 12c, at 0° heading angle, being very close for Optitrack and IMU.

The standard deviations among repetitions for the first mode frequency are minor and are not observable for some points. The damping factor is the less stable result, sensitive to the amplitudes taken, being standard deviation more representative. Differences in results from IMU and Optitrack data are less than 2% for frequencies in L14 and L12 position, Figs. 13a and 13b, being less than 3% for L01, Fig. 13c, specifically when the heading is 90° and 135°. Damping factor presented more significant variation for 135°, having a maximum error of 18.5%.

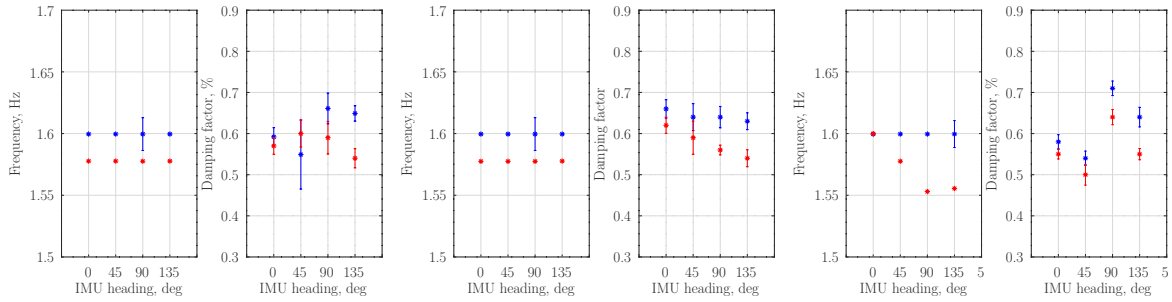


(a) L14. (b) L12. (c) L01.

Figure 12: Damped natural frequency and damping factor for IMU position, y-axis pointing up, IMU and Optitrack.

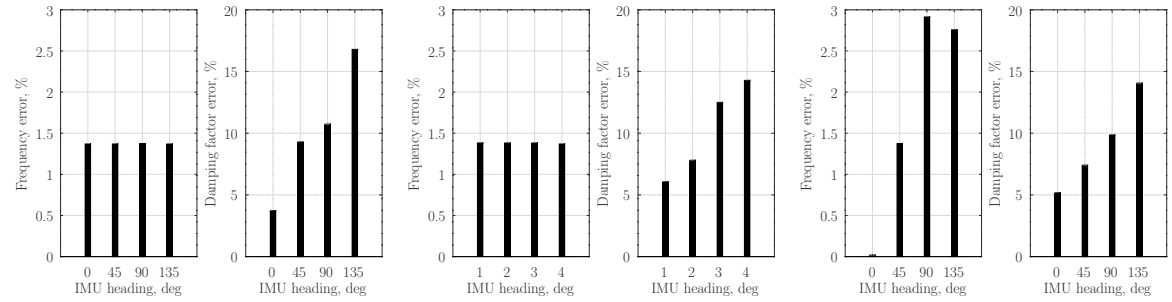


(a) L14. (b) L12. (c) L01.

Figure 13: First mode damped natural frequency and damping factor error for IMU position.

For the second mode (m2) frequency, values about 10.1 Hz were found using Optitrack and about 9.9 Hz using the IMU readings, which means a difference of approximately 2%. In fact, second mode displacement were very subtle and the maximum percentage error of 2.5%, see Fig. 14, is satisfactory for validation. Results for the y-axis pointing down were similar to y-axis pointing up and omitted due to redundancy of results.

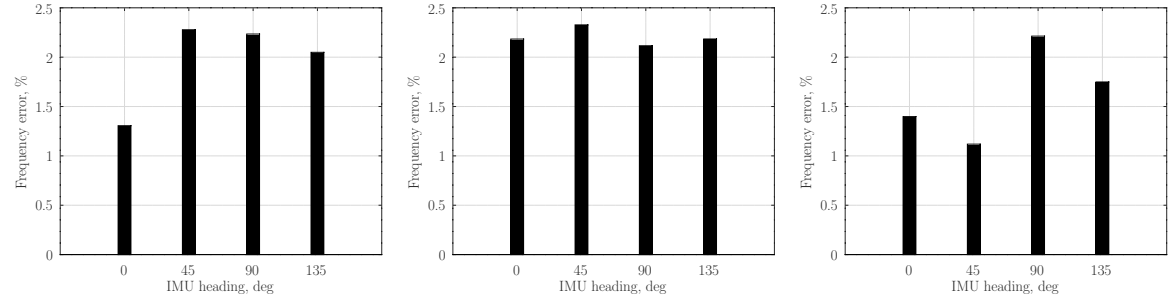


(a) L14. (b) L12. (c) L01.

Figure 14: Second mode damped natural frequency error for IMU position.

## 7. CONCLUSIONS

This work presented the methodology and results to validate a low-cost IMU using an optical tracking system, covering the calibration process, Kalman filter, Butterworth band-pass filter, quaternion rotation, and trapezoidal integration.

The systems are stable in time from the zero test values, with minimal differences in marker positions and IMU orientation over time.

Sensor-fusion using the Kalman filter removes the drift and high-frequency noise in Euler angles results, enabling proper coordinate rotation. Applying quaternion rotation, sixth order Butterworth filter, and trapezoidal integration to IMU accelerations is a good methodology to obtain displacement in a desired coordinate system once the results agree with the optical tracking system.

Damped natural frequencies, damping factor, and displacements along time can be computed independently the IMU position along tube length, orientation angle or axis direction. There are slight differences in the tube parameters between IMU and Optitrack, being less than 3% and 2.5% for first and second mode frequency, respectively. Errors are lower than 18.5% for damping factor. It is noted that these are percentage deviations for small damping values, calculated based on minimal displacement records as well, which denotes the relevance and good capacity of the IMU.

Results show that a low-cost IMU can be used for vibration analysis reliably, provided that signal analysis is performed. Now, the IMU is validated for use in VIV experiments in a test tank, that is, experiments with vibration forced by the fluid-structure interaction phenomenon of interest.

## 8. REFERENCES

Driessen, S.P., Janssen, N.H., Wang, L., Palmer, J.L. and Nijmeijer, H., 2018. "Experimentally Validated Extended Kalman Filter for UAV State Estimation Using Low-Cost Sensors". *IFAC-PapersOnLine*, Vol. 51, No. 15, pp. 43–48. ISSN 24058963. doi:10.1016/j.ifacol.2018.09.088.

Groves, P., 2013. *Principles of GNSS, Inertial, and Multisensor Integrated Navigation Systems, Second Edition*. GNSS/GPS. Artech House. ISBN 9781608070053.

Li, P., Cong, A., Dong, Z., Wang, Y., Liu, Y., Guo, H., Li, X. and Fu, Q., 2019. "Investigation on vortex-induced vibration experiment of a standing variable-tension deepsea riser based on bfbg sensor technology". *Sensors*, Vol. 19, No. 15, p. 3419.

McNeill, S., 2012. "Spectral formulations for vortex induced vibration modal decomposition and reconstruction". *Journal of offshore mechanics and Arctic engineering*, Vol. 134, No. 4.

Mukundan, H., Hover, F. and Triantafyllou, M., 2010. "A systematic approach to riser viv response reconstruction". *Journal of fluids and structures*, Vol. 26, No. 5, pp. 722–746.

Shi, C., Manuel, L. and Tognarelli, M., 2010. "Alternative empirical procedures for fatigue damage rate estimation of instrumented risers undergoing vortex-induced vibration". In *International Conference on Offshore Mechanics and Arctic Engineering*. Vol. 49149, pp. 911–922.

Titterton, D., Weston, J.L. and Weston, J., 2004. *Strapdown inertial navigation technology*, Vol. 17. IET.

Vissière, D., Martin, A. and Petit, N., 2007. "Using distributed magnetometers to increase IMU-based velocity estimation into perturbed area". *Proceedings of the IEEE Conference on Decision and Control*, pp. 4924–4931. ISSN 01912216. doi:10.1109/CDC.2007.4434809.

Zhang, H., Wu, Y., Wu, M., Hu, X. and Zha, Y., 2008. "A multi-position calibration algorithm for inertial measurement units". In *AIAA guidance, navigation and control conference and exhibit*. p. 7437.

## 9. RESPONSIBILITY NOTICE

The authors are solely responsible for the printed material included in this paper.